PNAS RESEARCH ARTICLE | BIOPHYSICS AND COMPUTATIONAL BIOLOGY

Temperature-dependent fold-switching mechanism of the circadian clock protein KaiB

Ning Zhang[a,1,2], Damini Sood[a,1,3], Spencer C. Guo[b,1], Nanhao Chen[c], Adam Antoszewski[b,4], Tegan Marianchuk[d], Supratim Dey[a,5], Yunxian Xiao[a], Lu Hong[d,6], Xiangda Peng[e], Michael Baxa[e], Carrie Partch[f], Lee-Ping Wang[c,7], Tobin R. Sosnick[e,7], Aaron R. Dinner[b,7], and Andy LiWang[a,g,7]

Affiliations are included on p. 8.

Edited by Jay Dunlap, Dartmouth College Geisel School of Medicine, Hanover, NH; received July 1, 2024; accepted October 24, 2024

The oscillator of the cyanobacterial circadian clock relies on the ability of the KaiB protein to switch reversibly between a stable ground-state fold (gsKaiB) and an unstable fold-switched fold (fsKaiB). Rare fold-switching events by KaiB provide a critical delay in the negative feedback loop of this posttranslational oscillator. In this study, we experimentally and computationally investigate the temperature dependence of fold switching and its mechanism. We demonstrate that the stability of gsKaiB increases with temperature compared to fsKaiB and that the Q10 value for the gsKaiB → fsKaiB transition is nearly three times smaller than that for the reverse transition in a construct optimized for NMR studies. Simulations and native-state hydrogen-deuterium exchange NMR experiments suggest that fold switching can involve both partially and completely unfolded intermediates. The simulations predict that the transition state for fold switching coincides with isomerization of conserved prolines in the most rapidly exchanging region, and we confirm experimentally that proline isomerization is a rate-limiting step for fold switching. We explore the implications of our results for temperature compensation, a hallmark of circadian clocks, through a kinetic model.

circadian clock | protein folding | molecular dynamics | NMR | temperature compensation

Significance

Circadian clocks foretell the coming of day and night in diverse organisms by preparing metabolic processes for sunrise and sunset. These ubiquitous systems are composed of proteins that undergo temporally separated protein–protein interactions and enzymatic reactions that reliably generate an internal representation of local time over a range of ambient temperatures (i.e., temperature compensation). Here, we use experiments and computations to characterize the temperature-dependent fold-switching behavior of the cyanobacterial circadian clock protein, KaiB. The free-energy landscape of KaiB changes with temperature in a way that may contribute to the overall mechanism of temperature compensation. Additionally, we find that proline *cis* ⇌ *trans* isomerization is a rate-limiting step in KaiB fold switching.

The fold of a protein is the i) overall three-dimensional arrangement of secondary structures (i.e., architecture) and ii) the path of the polypeptide chain through the structure (i.e., topology) (1). An exciting finding over the last several years is that some proteins do not follow the classic "one sequence, one fold" paradigm but can switch between different folds reversibly under physiological conditions (2, 3). These proteins belong to the relatively new class of so-called metamorphic proteins (4).

One of the most well-studied metamorphic proteins is KaiB, which is a core component of the oscillator of the cyanobacterial circadian clock (5). Circadian clocks are an adaptation to daily oscillations in ambient light and temperature and play important roles in the fitness and health in diverse organisms (6, 7). KaiB, together with KaiA, generates a circadian rhythm of phosphorylation in the clock protein KaiC to regulate downstream expression of clock-controlled genes (8).

In cyanobacteria with a circadian clock, KaiB exists in an equilibrium between two distinct folds with vastly different stabilities. The stable fold of KaiB with secondary structure βαββααβ is found only in KaiB homologs, and we refer to it as ground-state KaiB, or gsKaiB (9–12). The fold that binds KaiC is otherwise unstable; it is a thioredoxin-like fold with secondary structure βαβαββα, and we refer to it as fold-switched KaiB, or fsKaiB (Fig. 1). The much higher stability of gsKaiB relative to fsKaiB is the reason why the latter was not discovered until a decade after the structure of gsKaiB was solved by X-ray crystallography (5).

While fsKaiB is monomeric, gsKaiB self-associates to form dimers which in turn come together to form a homotetramer with C2 but not C4 symmetry. Thus, prior to binding KaiC, homotetramers of gsKaiB likely need to dissociate into monomers and then undergo a gsKaiB → fsKaiB fold switch (14, 15). Due to the instability of fsKaiB, it binds to KaiC slowly, on the hours time scale (16–18). Mutations that enhance the stability of fsKaiB relative to gsKaiB increase the rate of KaiB–KaiC binding but also abrogate clock function, suggesting that slowness of binding provides an important delay in the negative feedback loop of this clock (5). Each evening when fsKaiB binds KaiC, it inactivates KaiA (14, 16), displaces the sensor histidine kinase SasA from KaiC (16), activates the phosphatase activity of CikA (19), and binds the protein KidA, which tunes the period of the KaiABC oscillator (20). Thus, fsKaiB is a hub for nighttime signaling events.

Despite the importance of KaiB fold switching to the cyanobacterial circadian clock, much remains unknown about the mechanism of fold switching. Here, we describe

The authors declare no competing interest.

This article is a PNAS Direct Submission.

[1]N.Z., D.S., and S.C.G. contributed equally to this work.

[2]Present address: Qingdao Institute of Bioenergy and Bioprocess Technology, Chinese Academy of Sciences, Qingdao 266101, China.

[3]Present address: Department of Medicine, Duke University Medical Center, Durham, NC 27710.

[4]Present address: D. E. Shaw Research, New York, NY 10036.

[5]Present address: Feinberg School of Medicine, Northwestern University, Chicago, IL 60611.

[6]Present address: AbCellera, Vancouver, BC V5Y 0A1, Canada.

[7]To whom correspondence may be addressed. Email: leeping@ucdavis.edu, trsosnic@uchicago.edu, dinner@uchicago.edu, or aliwang@ucmerced.edu.

This article contains supporting information online at https://www.pnas.org/lookup/suppl/doi:10.1073/pnas.2412327121/-/DCSupplemental.

Published December 13, 2024.

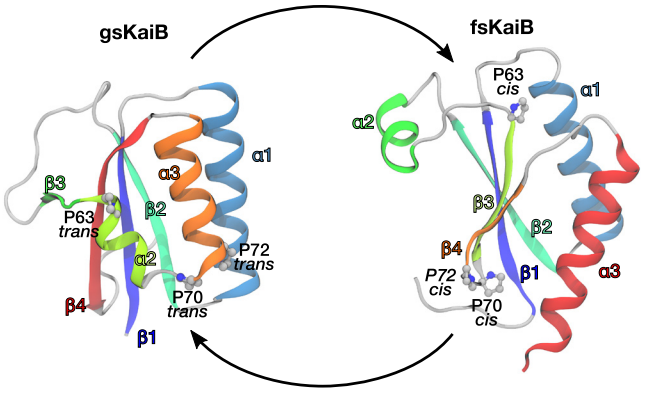

Fig. 1. KaiB switches reversibly between two distinct folds. Three proline residues—P63, P70, and P72—are *trans* in the ground-state fold of KaiB (gsKaiB, *Left*) and *cis* in the fold-switched fold of KaiB (fsKaiB, *Right*). PDB IDs 1VGL and 5JYT were used with VMD (13) to generate the ribbon diagrams for gsKaiB and fsKaiB, respectively.

experimental and computational evidence that the fold-switching thermodynamics and kinetics are sensitive to temperature. We then demonstrate that KaiB can undergo both partial and complete unfolding during fold switching and that isomerization of three conserved prolines located in a dynamic region of about ten residues is likely rate-limiting. We discuss the implications of our results for temperature compensation.

Results

The gsKaiB ⇌ fsKaiB Equilibrium Is Sensitive to Temperature. Our studies utilize KaiB from the thermophile *Thermosynechococcus elongatus (vestitus)* BP-1, but we expect the results to apply to KaiB from the widely studied mesophile *Synechococcus elongatus* PCC 7942 because they share 83% and 88% sequence identity and similarity, respectively, and the periods of the oscillators from both organisms are relatively insensitive to temperature (21, 22). Studying fold switching in wild-type (WT) KaiB is challenging because of the vastly different stabilities of the two folds and NMR peak doubling due to asymmetry in the homotetramer. Earlier, we found that truncating *T. elongatus* KaiB after residue 94 and introducing Y8A, D91R (or G89A), and Y94A amino acid substitutions shifts the gsKaiB ⇌ fsKaiB equilibrium to the right such that around room temperature the fsKaiB and gsKaiB states are similarly populated and monomeric (5) (*SI Appendix*, Figs. S1 and S2). Despite this change in stability, for clarity, we use the WT KaiB terms "ground state (gs)" and "fold-switched state (fs)" to refer to the matching folds of the KaiB mutants. Henceforth, we refer to *T. elongatus* KaiB 1-94 Y8A, D91R, Y94A as KaiB^{D91R} (and KaiB 1-94 Y8A, G89A, Y94A as KaiB^{G89A}).

We characterized the temperature dependence of the gsKaiB ⇌ fsKaiB equilibrium for KaiB^{D91R} (and KaiB^{G89A}). Size-exclusion chromatography indicated that the KaiB^{D91R} construct is monomeric at room temperature (*SI Appendix*, Fig. S3). ^{15}N,^{1}H heteronuclear single-quantum correlation (HSQC) NMR spectroscopy of ^{15}N-enriched KaiB^{D91R} (and KaiB^{G89A}) revealed that the gsKaiB ⇌ fsKaiB equilibrium is sensitive to temperature (Fig. 2*A*). ^{15}N,^{1}H HSQC spectra of KaiB^{D91R} (and KaiB^{G89A}) were collected at 20 °C, 25 °C, 30 °C, and 35 °C under equilibrium conditions, and ΔG values were estimated from the volume (population) ratios of the assignable peaks at each temperature (Fig. 2*B* and *SI Appendix*, Fig. S4*A*). Fitting the data to $\Delta G = \Delta H - T\Delta S$ shows that the gsKaiB ⇌ fsKaiB reaction is enthalpically driven ($\Delta H < 0$ and $\Delta S < 0$). Using the Protein Interactions Calculator (23), we compared intrachain contacts between gsKaiB (1VGL) and fsKaiB

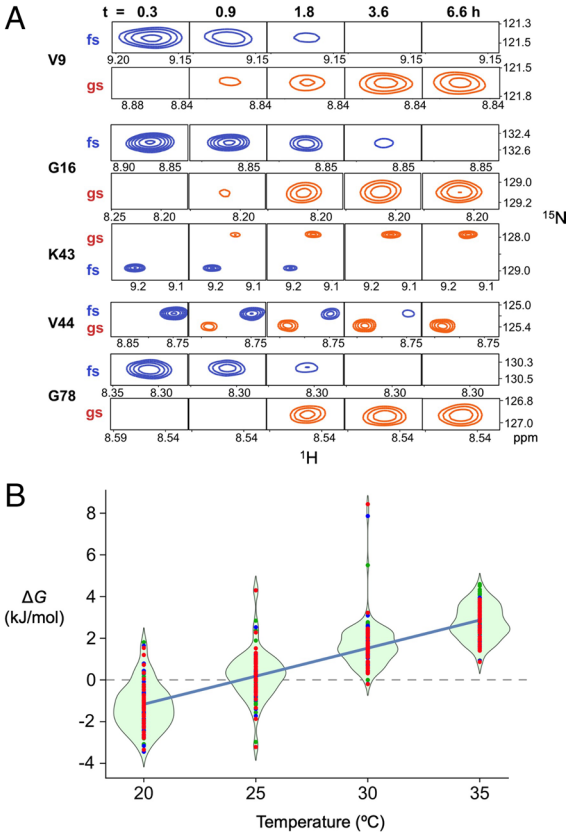

Fig. 2. The gsKaiB^{D91R} ⇌ fsKaiB^{D91R} equilibrium is sensitive to temperature. (*A*) A sample of ^{15}N-enriched KaiB^{D91R} was incubated at 4 °C for 24 h before inserting it into a 14.1 T NMR spectrometer that was set to 35 °C. ^{15}N,^{1}H HSQC spectra were collected over time and some representative regions are shown here. (*B*) Residue-specific ΔG values for the gsKaiB^{D91R} → fsKaiB^{D91R} reaction are plotted as red, green, and blue points, one color for each replicate, and are superimposed on distribution diagrams for each temperature sampled. The blue line is a fit to mean values using the equation $\Delta G = \Delta H - T\Delta S$. Fitting the data for individual residues yields $\Delta H = -82 \pm 18$ kJ mol^{-1} and $\Delta S = -276 \pm 58$ J mol^{-1} K^{-1}, indicating that the gsKaiB^{D91R} → fsKaiB^{D91R} reaction is enthalpically driven.

(5JWR), considering only residues in common between the two constructs and found that gsKaiB has approximately 16% more nonpolar contacts (and 8% fewer polar contacts).The change in polar and nonpolar solvent accessible surface areas for fsKaiB (5JWO, chain B, residues 7 to 94) and gsKaiB (1VGL, chain A, residues 7 to 94) as determined by the GETAREA method (*SI Appendix*, Table S1) (24) suggests moreover that $\Delta C_{p,\,gs\rightarrow fs} \approx$ 0.3 kJ mol^{-1} K^{-1} (25), which implies that the difference in heat capacities contributes no more than 5 kJ/mol to ΔH over the 20 to 35 °C range. We thus interpret the temperature dependence to result in part from the hydrophobic interactions weakening at low temperature (26, 27); this may also account for temperature-dependent fold switching of a designed protein (28).

The Activation Free Energies, $\Delta G^{\ddagger}_{gs\rightarrow fs}$ and $\Delta G^{\ddagger}_{gs\leftarrow fs}$, Have Opposite Temperature Dependencies. Next, we wanted to determine the extent to which the activation free energies for the forward and reverse fold-switching transitions, $\Delta G^{\ddagger}_{gs\rightarrow fs}$ and $\Delta G^{\ddagger}_{gs\leftarrow fs}$, respectively, are dependent on temperature. We incubated ^{15}N-enriched KaiB^{D91R} (and KaiB^{G89A}) at 4 °C for at least 24 h before collecting HSQC spectra as a function of time at 20 °C, 25 °C, 30 °C, and 35 °C. As shown in Fig. 3*A* for a representative residue, G16, we fit time-dependent changes in fractional populations using integrated volumes of assignable gsKaiB and fsKaiB HSQC peaks of ^{15}N-enriched KaiB^{D91R} (and KaiB^{G89A}) to obtain the observed rate of fold

switching, k_{obs}, upon a jump in sample temperature. For each temperature jump, the forward and reverse rate constants for fold switching, $k_{gs\to fs}$ and $k_{gs\leftarrow fs}$, were determined from k_{obs} and the equilibrium populations of gsKaiB and fsKaiB for each residue with an assignable set of HSQC peaks. These rate constants were used to calculate $\Delta G^{\ddagger}_{gs\to fs}$ and $\Delta G^{\ddagger}_{gs\leftarrow fs}$ using transition-state theory (see *SI Appendix* for details). As shown in Fig. 3*B* and *SI Appendix*, Fig. S4*B*, $\Delta G^{\ddagger}_{gs\to fs}$ increases, whereas $\Delta G^{\ddagger}_{gs\leftarrow fs}$ decreases with temperature. An equivalent perspective can be obtained by calculating Q10 = $k_{T+10\ °C}/k_T$, where k_T is the rate constant at temperature T (Fig. 3*C* and *SI Appendix*, Fig. S5). Using measurements at 25 °C and 35 °C, Q10 values for $k_{gs\to fs}$ and $k_{gs\leftarrow fs}$ are 2.1 ± 0.3 and 5.7 ± 0.8, respectively, for KaiB^{D91R}. Consequently, the rate of the gsKaiB → fsKaiB transition increases considerably less with temperature than the rate of the reverse reaction does. Temperature jumps from 40 to 20 °C, 25 °C, 30 °C, and 35 °C demonstrate that the temperature-dependent fold-switching behavior of KaiB^{D91R} (and KaiB^{G89A}) is reversible (*SI Appendix*, Figs. S6 and S7).

Simulations Reveal a Temperature-Dependent Fold-Switching Mechanism. To interpret these observations, we investigated how temperature affects fold-switching thermodynamics and kinetics using molecular dynamics (MD) simulations. While direct simulation of fold switching remains prohibitively costly, we were able to characterize KaiB's behavior by combining a machine-learned near-atomic resolution model, Upside (29), with a computational framework for estimating thermodynamics and kinetics from many short simulations that sample portions of the fold-switching transition (30, 31).

We simulated fold switching of KaiB^{D91R} at three temperatures ranging from a temperature where both gsKaiB and fsKaiB structures are stable to near the melting temperature (*SI Appendix*, *Upside Temperature Calibration*). The computed $\Delta G_{gs\to fs}$ was 3 to 6 k_BT (Fig. 4*A*), and gsKaiB is stabilized with respect to fsKaiB at higher temperatures, consistent with the experimental trend. The Upside $\Delta G_{gs\to fs}$ values are somewhat larger than the experimentally observed ones. For comparison, we also used all-atom MD simulations to compute the temperature dependence of the fold-switching free energy difference from the temperature dependence of the free energy of each individual fold (*SI Appendix*). The relative stabilization from these simulations was approximately 4 kJ/mol (*SI Appendix*, Fig. S8), consistent with the experimental findings. Based on this comparison, we infer that the Upside temperature range is somewhat higher and broader than that studied experimentally.

Our analysis for the Upside simulations enables us to compute an important statistic for dissecting the fold-switching mechanism: the probability of reaching the fsKaiB state before the gsKaiB state from a given conformation (q). This statistic serves as a measure of progress (i.e., reaction coordinate), and we define the transition state as q = 0.5. We interpret q structurally using the fraction of native contacts (32) in the N-terminal half of the protein (Q_N) and the difference in the fractions of gsKaiB and fsKaiB C-terminal contacts ($Q_{fs,C} - Q_{gs,C}$; *SI Appendix*, Table S2). The transition state cuts diagonally at $Q_{fs,C} - Q_{gs,C} \approx 0.5$ (*SI Appendix*, Fig. S9) and shifts toward the fsKaiB state as the temperature increases, consistent with the Hammond postulate (33–35).

Potentials of mean force (free energies) as functions of these coordinates are shown in Fig. 4*A* and *SI Appendix*, Fig. S10. There is a barrier between the unfolded intermediates and the fsKaiB state, consistent with the location of the transition state, as well as metastable intermediates at ($Q_{fs,C} - Q_{gs,C}$, Q_N) ≈ (–0.6, 0.6), (0.0, 0.4), (0.0, 0.0), and (0.7, 0.5), for which we show selected structures (Fig. 4*B*). Structures with the C-terminal half folded and the N-terminal half unfolded are too high in free energy to be observed, as indicated by the absence of points in the lower left and right corners of the plots in Fig. 4*A*.

The intermediates marked with a square, star, and circle are on the fold-switching pathway, corresponding to gain or loss of individual C-terminal secondary structures. We show potentials of mean

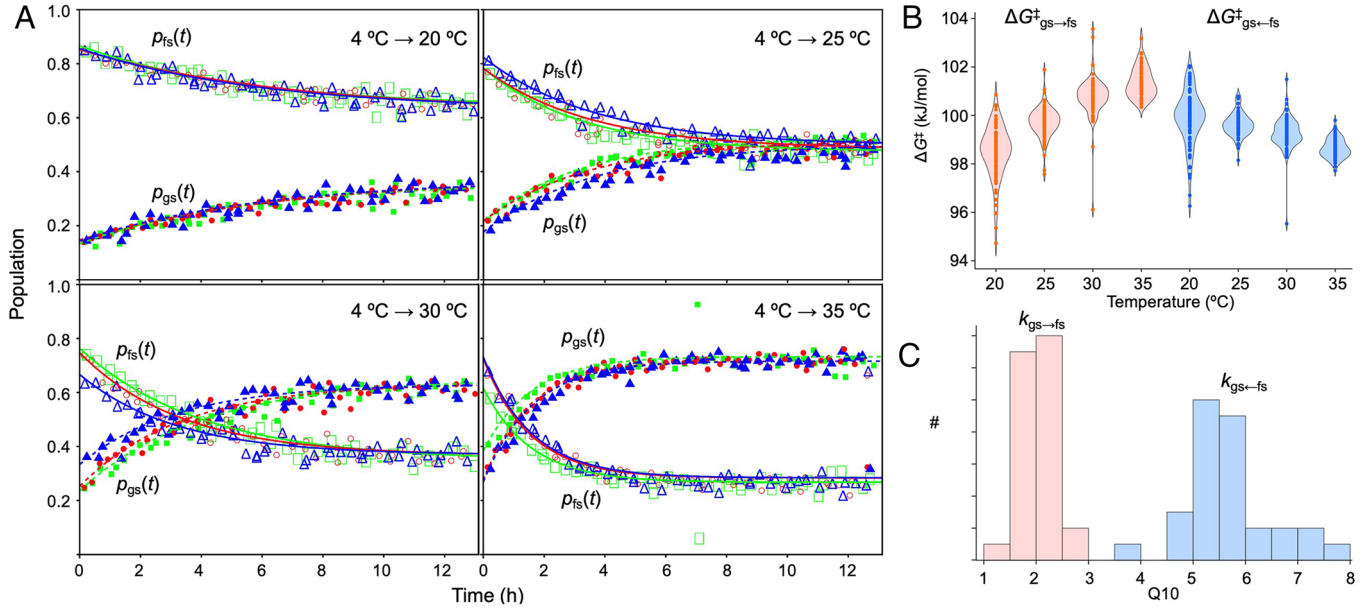

Fig. 3. The kinetics of gsKaiB^{D91R} → fsKaiB^{D91R} and gsKaiB^{D91R} ← fsKaiB^{D91R} fold switching differ in their dependence on temperature. (*A*) Kinetics of gsKaiB^{D91R} ← fsKaiB^{D91R} fold switching of residue G16 under different temperature jumps. A sample of ^{15}N-enriched KaiB^{D91R} was incubated at 4 °C for at least 24 h before inserting it into a 14.1 T NMR spectrometer that was set at either 20 °C, 25 °C, 30 °C, or 35 °C. ^{15}N,^{1}H HSQC spectra were collected at regular intervals after a dead time of approximately 4 min. Open and solid symbols represent fractional populations of residue G16 in the gsKaiB^{D91R} and fsKaiB^{D91R} folds, respectively. Red, green, and blue colors represent separate experiments, each of which used a freshly prepared sample. HSQC peak volumes were determined by nmrPipe and nmrDraw. (*B*) $\Delta G^{\ddagger}_{gs\to fs}$ and $\Delta G^{\ddagger}_{gs\leftarrow fs}$ as a function of temperature for all residues, and (*C*) histograms of residue-specific Q10 values for $k_{gs\to fs}$ and $k_{gs\leftarrow fs}$. The forward and reverse reactions are rendered in pink and blue, respectively. In (*B*) and (*C*) the three replicates were pooled. Residue-specific plots of Q10 values are presented in *SI Appendix*, Fig. S5.

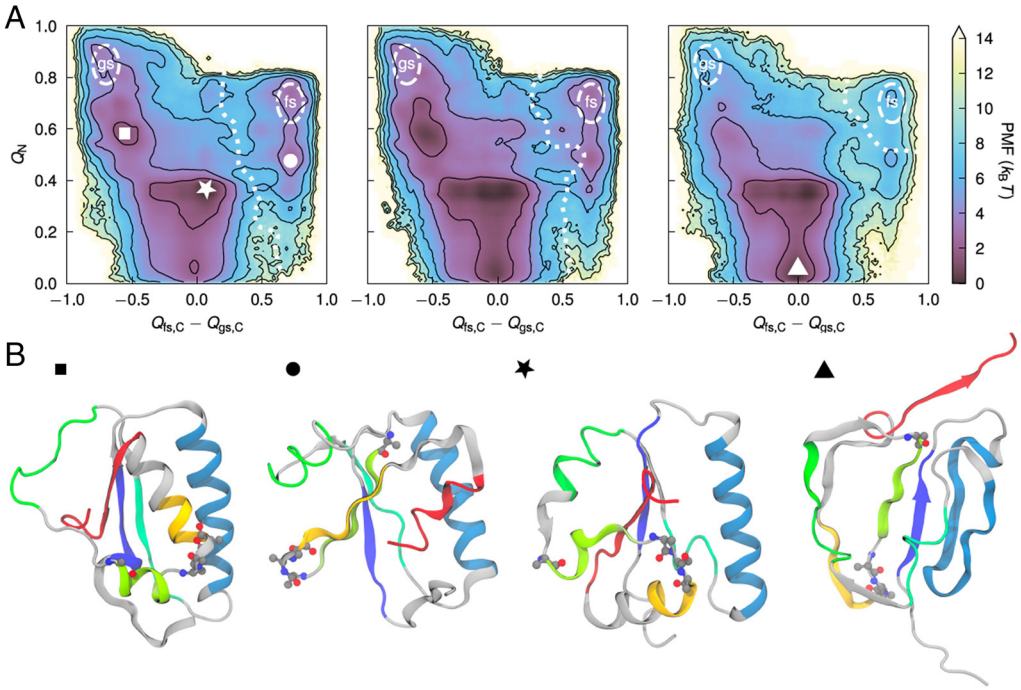

Fig. 4. Fold switching in an Upside model of KaiB^{D91R} involves partially and completely unfolded intermediates. (*A*) Potential of mean force as a function of the fraction of N-terminal contacts (Q_N) and the difference in the fractions of gsKaiB and fsKaiB C-terminal contacts ($Q_{fs,C} - Q_{gs,C}$). From *Left* to *Right*, the Upside temperature is increasing. Contour lines are drawn every 2 k_BT. The approximate location of the transition state ($q = 0.5$) is marked as a dashed line. (*B*) Selected structures corresponding to points marked on the potentials of mean force in (*A*). The sequence is colored by the position of secondary structures in fsKaiB and P63, P70, P71, and P72 are shown as balls and sticks.

force as functions of collective variables characterizing individual secondary structure transitions (*SI Appendix*, *Collective Variables*) in *SI Appendix*, Fig. S11. The presence of multiple minima in these plots indicates that these secondary structures can generally transition independently. At the same time, the diagonal symmetry of the $Q_{fs,\beta4} - Q_{gs,\alpha3}$ and $Q_{fs,\beta3} - Q_{gs,\alpha2}$ plot (*SI Appendix*, Fig. S11*A*) suggests that the $\alpha2_{gs} \rightleftarrows \beta3_{fs}$ and $\alpha3_{gs} \rightleftarrows \beta4_{fs}$ regions form the $\beta3_{fs}/\beta4_{fs}$ sheet together, while the lack of an intermediate at (1, –1) in the $Q_{fs,\beta4} - Q_{gs,\alpha3}$ and $Q_{fs,\alpha3} - Q_{gs,\beta4}$ plot (*SI Appendix*, Fig. S11*B*) suggests that $\beta4_{gs}$ switches to $\alpha3_{fs}$ before $\alpha3_{gs}$ switches to $\beta4_{fs}$ (and $\alpha2_{gs}$ switches to $\beta3_{fs}$). The intermediate marked with a triangle in Fig. 4 is off-pathway and corresponds to complete unfolding of the N-terminal half of the protein. As one would expect, increasing the temperature stabilizes this intermediate.

The picture that emerges is that fold switching can proceed via pathways where the C-terminal half of the protein is unfolded while the N-terminal half is unfolded to varying degrees, with higher temperatures favoring a completely unfolded intermediate. Because this intermediate is on the gs side of the transition state ($q \leq 0.3$, *SI Appendix*, Fig. S9), the reactive flux for fold switching involving this intermediate (*SI Appendix*, *Reactive Flux through Unfolded State*) decreases from 75 to 60% in the gs → fs direction as temperature increases, while the opposite is true for the gs ← fs direction (i.e., in both cases, the system tends toward the intermediate and, in turn, gsKaiB as temperature increases, *SI Appendix*, Fig. S10). Given that the Upside temperature range is likely higher than the experimental one, as noted above, the global unfolding pathway may be overemphasized by the Upside simulations. Nevertheless, they suggest that KaiB can transition by either partial or complete unfolding.

Hydrogen–Deuterium Exchange (HDX) Experiments and Simulations Are Consistent with Large-Scale Unfolding for a fs Variant of KaiB. To test the predictions of the simulations that KaiB can transition by either partial or complete unfolding, we probed fsKaiB's free energy surface with native-state HDX experiments. HDX experiments performed on proteins under equilibrium conditions can provide insights into regions of proteins that undergo thermally induced local, larger-scale partial, and complete unfolding events by quantifying the sensitivity of HDX rates to the addition of low-to-moderate amounts of denaturant (36). HDX rates of residues whose exchange is determined by local unfolding events can be identified by their having minimal denaturant dependence while the rates of residues that undergo HDX upon larger-scale partial or complete unfolding events have higher sensitivity (larger *m*-values).

Although we wanted to carry out HDX experiments on KaiB^{D91R}, not all peaks in the HSQC spectrum for the α2-β3-β4 region could be assigned. Therefore, we created a construct for HDX experiments that is more stable in the fsKaiB fold—*T. elongatus* KaiB 1-99 Y8A P71A G89A D91R Y94A—hereafter fsKaiB^{HDX}. For this variant, resonances in the α2-β3-β4 region were assignable. The destabilizing P71A substitution was incorporated so that the construct was more sensitive to the low concentrations of urea used here. We measured HDX rates at 50+ sites at pH 5.5 and 30+ sites at pH 6.5 at urea concentrations of 0, 0.5, 1.0, 1.5, 2.0, and 2.5 M urea. The most stable regions were associated with the β1-α1-β2 and α3 regions, which exchanged ~10 to 100 times slower than the α2-β3-β4 region. This difference indicates that, of four segments that switch secondary structures, three (α2, β3, and β4) are much less stable and/or have faster opening rates than the fourth fold-switching segment (α3).

Additionally, the HDX rates for β1-α1-β2 and α3 exhibited a common and larger urea dependence than the less stable α2-β3-β4 region (Fig. 5 and *SI Appendix*, Fig. S12). These observations suggest that HDX for sites within β1-α1-β2 and α3 occurs through large-scale unfolding events involving unfolding of the whole protein (although the α3 helix may have some residual helical structure as HDX rates in this helix are ~2× slower than in the β1-α1-β2 region). In contrast, the fold-switching residues across the α2-β3-β4 region undergo more frequent unfolding events.

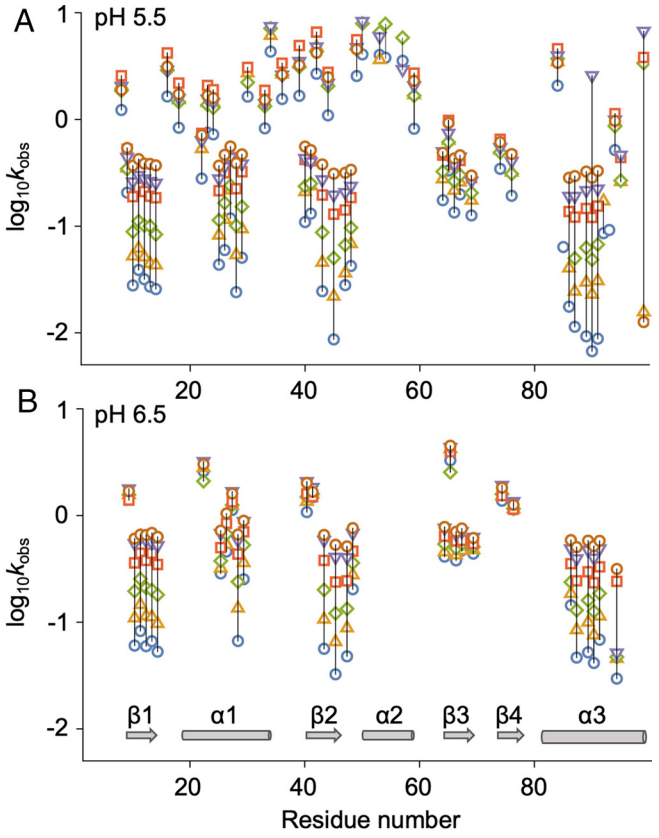

Fig. 5. HDX rates for KaiB^{HDX} indicate that β1-α1-β2 and α3 are more stable than α2-β3-β4. Observed exchange rates ($\log_{10}$ of k_{obs} in h^{-1}) at (*A*) pH 5.5 and (*B*) pH 6.5. In (*A*) and (*B*), blue circles, gold triangles, green diamonds, red squares, inverted purple triangles, and brown circles represent data in 0.0, 0.5, 1.0, 1.5, 2.0, and 2.5 M urea, respectively. Each data point represents the mean of two replicates, except for those at 2.0 M urea at pH 5.5 and 1.5 M urea at pH 6.5, for which there was only one measurement. The SE in the mean was 0.05 on average for datasets at both pH values. Residues with a measurable k_{obs} value at only a single urea concentration were not included in these plots. The secondary structure cartoons along the *Bottom* of (*B*) represent the fold-switched structure.

A rigorous interpretation of HDX rates requires the determination of the extent to which exchange reflects the kinetics or thermodynamics of the opening events, termed the EX1 or EX2 limits, respectively (37). Observed HDX rates, k_{obs}, generally depend on relative rates of opening (unfolding), k_{op}, closing (refolding), k_{cl}, and exchange with solvent for an exposed amide proton, k_{chem}:

$$\mathrm{N{-}H\cdots O{=}C} \underset{k_{cl}}{\overset{k_{op}}{\rightleftharpoons}} \mathrm{N{-}H + O{=}C} \xrightarrow{k_{chem}} \mathrm{N{-}D + O{=}C}.$$

When $k_{chem} >> k_{cl}$, the system is in the EX1 limit and the HDX rate is given by $k_{obs} = k_{op}$. Conversely, when $k_{chem} << k_{cl}$, the system is in the EX2 limit and $k_{obs} = k_{chem}/PF$, where $PF = K_{eq}+1$ is the protection factor and $K_{eq} = k_{op}/k_{cl}$. As discussed in *SI Appendix*, the exchange behavior for KaiB^{HDX} falls in a mixed EX1-EX2 regime, which complicates interpretation and prevents direct comparison to simulations.

Nevertheless, the patterns in Fig. 5 described above are mirrored by site-resolved hydrogen-bond stabilities calculated from Upside simulations of ground-state dynamics of the KaiB^{HDX} construct assuming an EX2 limit (*SI Appendix*, Fig. S12). Despite the actual exchange being in a mixed EX1-EX2 regime, we consider the HDX data consistent with the Upside model in that they both support a scenario where the α2-β3-β4 region undergoes unfolding much more frequently than the non-fold-switching region, β1-α1-β2.

However, one of the fold-switching elements, the α3 helix, is much more stable than the other three and even has dynamics matching the stable, non-fold-switching region. This unexpected finding argues that the free energy surface does not have a stable intermediate that contains only the N-terminal (non-fold switching) half of the protein, at least in the case of KaiB^{HDX}, which was engineered to be monomeric by stabilizing α3 in the fs fold at the expense of β4 in the gs fold. This finding is consistent with the significant fluxes through the completely unfolded intermediate in the Upside simulations of KaiB^{D91R}. Nevertheless, both the simulations and experiments suggest there are also fold-switching pathways in which α2-β3-β4 region unfolds with the rest of the protein intact.

Proline Isomerization Is the Rate-Determining Step for KaiB^{D91R} Fold Switching. KaiB^{D91R} switches fold on the same hours time scale as KaiB–KaiC binding, whereas KaiB mutants locked in the fsKaiB fold by mutagenesis bind to KaiC instantaneously (5). The faster binding also abrogates clock function, suggesting that slow KaiB–KaiC binding provides an essential delay in the negative-feedback arm of the oscillator. The sensor histidine kinase, SasA, binds KaiC much faster than KaiB does because its N-terminal KaiC-binding domain is constitutively in the fsKaiB (thioredoxin-like) fold (8, 38). This much faster binding allows the SasA–KaiC complex to activate the master transcription factor, RpaA, by phosphorylation before KaiB–KaiC binding displaces SasA, creating circadian rhythms of gene expression.

Given the biological significance of the kinetics of KaiB fold switching, we wanted to identify the rate-determining step of fold switching. A key feature of the α2-β3-β4 region that more readily undergoes HDX is that it contains three prolines (P63, P70, and P72) that are *trans* in gsKaiB and *cis* in fsKaiB. Given that proline isomerization has previously been implicated in controlling protein conformational changes (39–41), and that its time scales and activation free energies (42–44) are similar to those of KaiB^{D91R} fold switching (Fig. 3*B*), we asked whether proline isomerization is the rate-determining step for fold switching.

We found in the aforementioned Upside simulations that P63, P70, and P72 remain *trans* nearly 100% of the time in gsKaiB but are *cis* less than 30% of the time in fsKaiB. Moreover, P71, which experimentally is *trans* in both gsKaiB and fsKaiB, populates the *cis* isomer 90% of the time in simulations of fsKaiB (*SI Appendix*, Table S3). These deviations from experimental observations likely result from Upside representing the proline *cis* and *trans* states through a double-well potential without accounting for side chain steric hindrance, so we interpret P70 to P72 as acting as a single unit in the Upside model of KaiB^{D91R}.

With this limitation of our model in mind, we probe the structural changes associated with proline isomerization. The *cis* fraction of P63 and any of P70 to P72 rises sharply when $Q_{fs,C} - Q_{gs,C} \approx 0.5$ (*SI Appendix*, Fig. S13 *A* and *B*), near the transition state for fold switching (*SI Appendix*, Fig. S9). However, the P70 to P72 isomerization appears less temperature sensitive and less dependent on the Q_N value, which suggests that it does not require global unfolding. Rather, consistent with the location of P70–P72 in the sequence, their isomerization occurs with the packing of the two C-terminal β-strands, β3 and β4, in the fsKaiB state (*SI Appendix*, Fig. S13*C*).

To probe whether isomerization of P63, P70, and P72 (with P71 in the *trans* state) is sufficient to induce fold switching computationally, we altered the conformations of P63, P70, and P72 in the

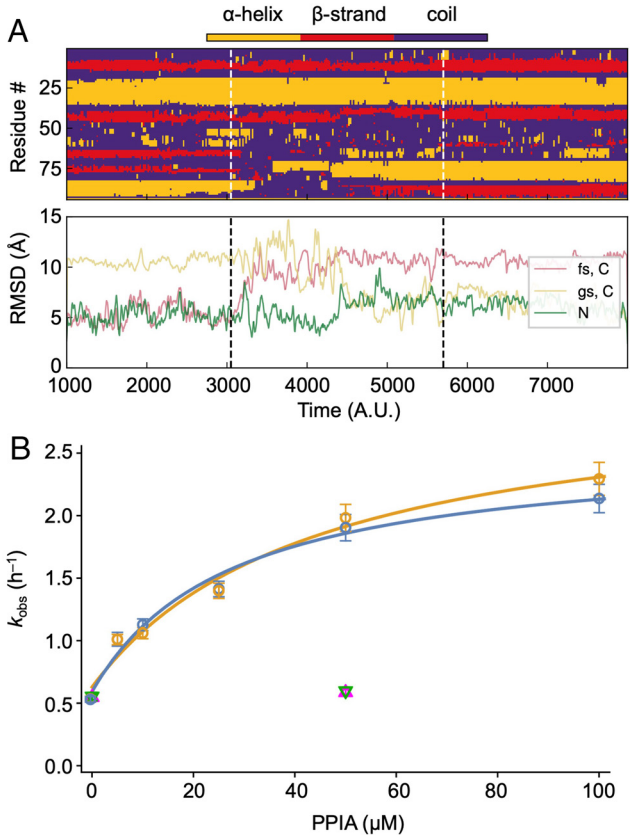

Fig. 6. Proline isomerization is rate-limiting for gsKaiB ← fsKaiB fold-switching of KaiB^{D91R}. (*A*) An Upside simulation starting from fsKaiB with P63, P70, and P72 fixed in *trans*. (*Top*) Secondary structure assigned via DSSP (46) and (*Bottom*) RMSD to either the C-terminal half of fsKaiB, the C-terminal half of gsKaiB, or the N-terminal half (*SI Appendix*, Table S2) during a section of a successful fold-switching trajectory from fsKaiB to gsKaiB. RMSDs are plotted as a moving average over 20 frames. The dotted lines indicate the approximate start and end times of the fold-switching event. (*B*) Observed rates of fold switching, k_{obs}, after a jump to 35 °C for KaiB^{D91R} samples pre-equilibrated at 4 °C as a function of the concentration of human PPIA. 190 to 200 μM ^{15}N-enriched KaiB^{D91R} samples stored at −80 °C were incubated at 4 °C for 24 h before inserting them into the NMR spectrometer, which was set to a sample temperature of 35 °C. ^{15}N,^{1}H HSQC spectra were collected every 18 min over a span of 7 h. Residue-specific rates were determined from these spectra as described in *SI Appendix*. Circles represent k_{obs} values from globally fitting data from residues with resolved and assigned gsKaiB and fsKaiB HSQC peaks (35 residues total). Replicates are depicted in different colors (blue and gold). Triangles represent k_{obs} values where 55 μM cyclosporin A (CsA) was added to the samples. Replicates are depicted in different colors (green and pink). Error bars represent uncertainties from the global fits.

fsKaiB structure from *cis* to *trans* and ran simulations of KaiB^{D91R} with each proline locked in its assigned conformer (i.e., subjected to a single-well potential for backbone isomerization). From 240 such simulations (the simulation temperature was set to 0.89 for 144 trajectories or 0.90 for 96 trajectories relative to a melting temperature of 0.94), we observed four transitions to gsKaiB, all of which involved partial (and not complete) unfolding (Fig. 6*A* and *SI Appendix*, Fig. S14). In these simulations, the transition tends to start with the unfolding of $\beta3_{fs}$ and $\beta4_{fs}$, which may give the proline(s) freedom to isomerize; the remaining steps involve $\alpha3_{fs}$ unfolding followed by folding of $\alpha3_{gs}$ and either $\beta4_{gs}$ or $\alpha2_{gs}$. 384 analogous simulations (192 at each temperature) starting in the gsKaiB state with P63, P70, and P72 locked in *cis* did not yield any fold-switching events to the fsKaiB state for KaiB^{D91R}. This difference could reflect the relative stability of the gsKaiB state for the KaiB^{D91R} mutant compared to the fsKaiB state [by contrast, KaiB^{G89A} displayed both gs → fs and gs ← fs transitions during analogous Upside simulations (45)]. Nonetheless, our observation of proline isomerization-induced gs ← fs fold-switching events with partial unfolding indicates that complete unfolding is not required for fold switching, despite the observations in the unbiased simulations reported above.

To verify the computational prediction that proline isomerization is a key step in fold switching, we modulated the barrier to proline isomerization using human peptidyl prolyl isomerase A [PPIA, also known as cyclophilin A or CypA (47)], which is a member of the cyclophilin family. PPIA enhanced the rate of KaiB fold switching in a dose-dependent manner as measured by NMR (Fig. 6*B*), and cyclosporin A, an inhibitor of cyclophilins (47), abolished the effect of PPIA, suggesting that proline isomerization indeed contributes significantly to the slowness of fold switching. Given that prolyl isomerases such as PPIA likely bind to prolines in unstructured segments (40, 48, 49), unfolding of $\beta3_{fs}$ and $\beta4_{fs}$ probably precedes proline isomerization, consistent with the simulations, and possibly contributes to the overall rate of fold switching as the rate enhancement by PPIA is rather modest (*SI Appendix*, Fig. S15). Our simulations and experiments do not resolve whether any of the three isomerizing proline residues plays a dominant role. Nevertheless, they suggest that it is the combination of unfolding and proline isomerization that makes KaiB fold switching slow.

Discussion

Over the last couple decades, there has been a dramatic breakdown in the traditional one-to-one-to-one relationship between sequence, fold, and function of proteins. Not only are there intrinsically disordered proteins (50), some of which fold upon binding, but also amyloid proteins and prions, which can change their folds but do so irreversibly (51). Metamorphic proteins like KaiB, which can populate two well-folded structures reversibly, have received much less attention. They are distinct from morpheeins, which are proteins that adopt different quaternary structures while retaining the same fold (52), and moonlighting proteins, which have more than one biochemical function but the same fold (53). It remains to determine how many metamorphic proteins in the Protein Data Bank are masquerading as single-fold (or monomorphic) proteins (2, 54–56). Our work aids in this effort by providing insights into the forces that mediate fold switching.

Our simulations and native-state HDX data on KaiB^{HDX} suggest that it switches folds via both partially and completely unfolded pathways, with the α2-β3-β4 region of fsKaiB exhibiting the greatest lability. These mechanistic findings can be linked to our temperature studies through the observation that electron-spin resonance experiments on *T. elongatus* KaiB labeled at different positions with paramagnetic probes indicate that internal motions in the α2 region of the gsKaiB fold are particularly sensitive to temperature (57). These residues are at a monomer–monomer interface in the WT KaiB homotetramer. Given that oligomerization requires KaiB to be in the gsKaiB fold (10, 11), our finding that an increase in temperature stabilizes gsKaiB relative to fsKaiB may explain the observation that a mutant of *T. elongatus* KaiB with the first nine residues deleted is a dimer at 35 °C but a monomer at 4 °C (58); we similarly interpret the observation that lower temperature favors formation of the KaiABC complex (59). However, it bears noting that our model of KaiB fold switching may not precisely describe the behavior of WT KaiB. For example, our finding that proline isomerization is rate limiting for fold switching was obtained for a monomeric construct (KaiB^{D91R}) whereas oligomerization was determined to be rate limiting for WT KaiB, as suggested by a computed thermodynamic cycle and structure-based modeling (15). On the other hand, we note that slow conformational switching in the protein BMAL1, which

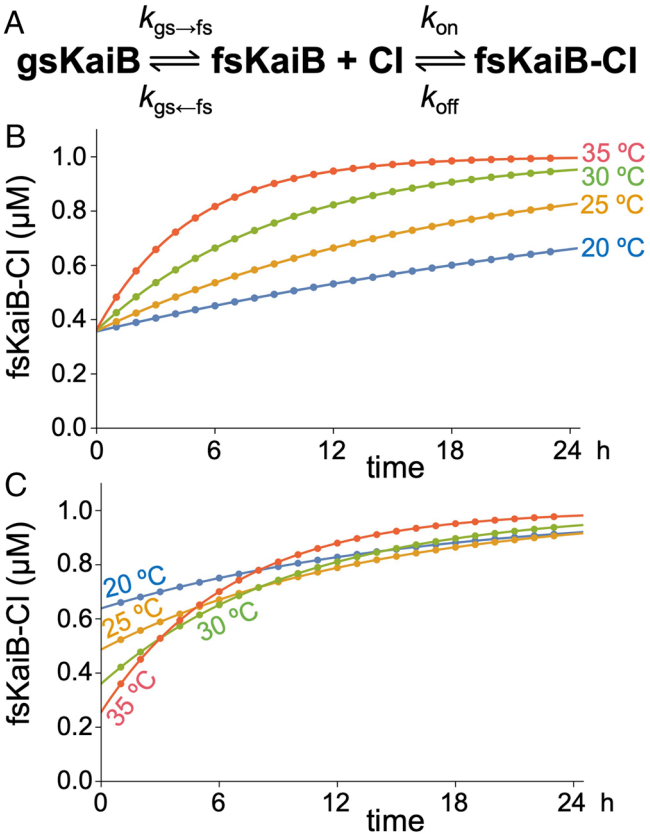

Fig. 7. Kinetics of formation of the fsKaiB^{D91R}–CI complex is partially temperature compensated. (*A*) Reaction scheme of KaiB^{D91R} fold switching and binding the CI domain of KaiC. (*B*) Calculated kinetics of fsKaiB^{D91R}–CI complex formation when ΔG and $\Delta G^{\ddagger}$ values are fixed at their experimentally determined 30 °C values. (*C*) Calculated kinetics of fsKaiB^{D91R}–CI complex formation using ΔG and $\Delta G^{\ddagger}$ values experimentally determined at each temperature modeled.

plays significant roles in timekeeping by the mammalian circadian clock, requires proline isomerization and is modulated by isomerases of the cyclophilin family (39).

In the Protein Data Bank, the gsKaiB fold is found only in KaiB homologs, whereas the fsKaiB thioredoxin-like fold is common. Thus, it is plausible that ancestors of KaiB adopted the thioredoxin-like fold exclusively and later evolved the ability to reversibly switch to the gsKaiB fold for the purpose of circadian timekeeping. For example, the Kai system in *Rhodobacter sphaeroides* functions as an hourglass timer rather than a self-sustaining clock, and its KaiB can adopt both the gsKaiB and fsKaiB states (54, 60). In contrast, the bacterium *Legionella pneumophila*, which is not known to possess a circadian clock, has a *kaiBC* operon where the KaiB protein crystallizes in the thioredoxin-like fsKaiB fold and has an alanine residue at position 89 as KaiB^{G89A} does (61).

By controlling KaiBC complex formation (5, 18, 62), KaiB fold switching i) contributes to the slowness of the circadian clock, ii) provides time-delayed negative feedback essential to all biochemical oscillators (63), and iii) opens a transient window of RpaA activation by allowing SasA to bind to the CI domains of KaiC before KaiB does (8). KaiB assembles as a hexameric ring onto the post-ATP hydrolysis state of the CI ring at night (14, 59, 60), displaces SasA (16), sequesters an autoinhibited state of KaiA (14, 59), and separately binds CikA, which then dephosphorylates RpaA. When bound to KaiC, KaiB also interacts with the protein KidA to tune the period of the cyanobacterial circadian oscillator (20). Thus, fold switching by KaiB is essential to multiple aspects of clock function.

A remarkable feature of circadian clocks is that their amplitudes change so that their periodicities are relatively insensitive to temperature (64–67). This temperature compensation enables circadian clocks to reliably maintain an internal representation of time. For cyanobacteria, it is well established that the ATPase activity of KaiC is temperature compensated (66, 68). The temperature shifts that we observe for the gsKaiB ⇌ fsKaiB equilibrium should also contribute to temperature compensation of the cyanobacterial circadian clock. To illustrate this, we used a simple reaction scheme to model the binding kinetics between KaiB^{D91R} and the CI domain of KaiC (Fig. 7*A*). This model can be described by the following coupled differential equations (see *SI Appendix* for details):

$$\frac{d\left[\text{gsKaiB}^{D91R}\right]}{dt} = -k_{gs\rightarrow fs}\left[\text{gsKaiB}^{D91R}\right] + k_{gs\leftarrow fs}\left[\text{fsKaiB}^{D91R}\right],$$

$$\frac{d\left[\text{fsKaiB}^{D91R}\right]}{dt} = k_{gs\rightarrow fs}\left[\text{gsKaiB}^{D91R}\right] - k_{gs\leftarrow fs}\left[\text{fsKaiB}^{D91R}\right] - k_{on}\left[\text{fsKaiB}^{D91R}\right][\text{CI}] + k_{off}\left[\text{fsKaiB}^{D91R}\text{:CI}\right].$$

In Fig. 7*B*, we calculated the kinetics of fsKaiB^{D91R}–CI complex formation as a function of temperature but with ΔG and $\Delta G^{\ddagger}$ fixed at values experimentally determined at 30 °C. In contrast, for Fig. 7*C* we used values determined experimentally for each temperature modeled. As can be seen for both cases, higher temperatures lead to faster binding. However, for the temperature-dependent case, the amounts of fsKaiB^{D91R}–CI complex formed across the different temperatures are more similar, because with increasing temperature the gsKaiB^{D91R} ⇌ fsKaiB^{D91R} equilibrium shifts toward gsKaiB^{D91R}, and $\Delta G^{\ddagger}_{gs\rightarrow fs}$ and $\Delta G^{\ddagger}_{gs\leftarrow fs}$ increase and decrease, respectively (*SI Appendix*, Fig. S15). The temperature dependence of the KaiB free-energy landscape in the circadian system of *R. sphaeroides* has similarities with the behavior of KaiB^{D91R} (69). We speculate that KaiB fold switching likely contributes to the overall mechanism of temperature compensation in the cyanobacterial circadian clock and perhaps also in *R. sphaeroides*. Interestingly, the cyanobacterial circadian clock can also compensate for changes in molecular crowding (70), which not only impacts complex formation but also shifts the gsKaiB ⇌ fsKaiB reaction to the left (71). Mechanistic studies of the interplay between clock complex formation and fold switching under various conditions would be worthwhile.

Materials and Methods

Cloning, Protein Expression, and Purification. KaiB constructs are listed in *SI Appendix*, Table S4 and were expressed and purified using previously published methods (72, 73). Briefly, cells were grown to $OD_{600} \approx 0.6$ in M9 medium containing ^{15}N-labeled ammonium chloride (Cambridge Isotope Laboratories, Inc.) and induced by adding isopropyl β-*d*-1-thiogalactopyranoside to a final concentration of 200 μM for 12 h at 30 °C. Cells were harvested and cell pellets were resuspended using 4 °C lysis buffer (50 mM NaH_2PO_4, 500 mM NaCl, pH 8.0) and homogenized with an Avestin C3 Emulsiflex homogenizer (Avestin Inc, Canada). Supernatant was clarified by centrifugation, loaded onto a Ni-NTA column (QIAGEN, #30230), and the column was washed with a buffer solution (50 mM NaH_2PO_4, 500 mM NaCl, 20 mM imidazole, pH 8.0). His-tagged KaiB was eluted with a buffer solution consisting of 50 mM NaH_2PO_4, 500 mM NaCl, and 250 mM imidazole, pH 8.0. His-tagged ULP1 protease was added to His-tagged KaiB to final concentration of 3 μM and the sample was incubated for 12 h followed by loading 10×-diluted sample onto a Ni-NTA column to remove ULP1 and the SUMO tag. The flowthrough containing KaiB was then passed through a HiLoad 16/600 Superdex 75 size-exclusion column in phosphate buffer (20 mM Na_2HPO_4/NaH_2PO_4, 100 mM NaCl, pH 7.0) by FPLC. Finally, protein purity was assessed by SDS PAGE. All KaiB samples were stored at −80 °C.

Analytical Gel-Filtration Chromatography. A Superdex™ 75 Increase 10/300 GL column (Cytiva) with an injection volume of 100 μL was used for analytical gel-filtration chromatography of KaiB samples in SEC buffer (20 mM Na_2HPO_4/NaH_2PO_4, 100 mM NaCl, pH 7.0). Samples were incubated at 4 °C overnight (~12 h) and then injected onto the column with a flow rate of 0.7 mL/min.

NMR Temperature-Jump Experiments. NMR experiments were performed on a Bruker Avance III 600 MHz spectrometer equipped with a TCI cryoprobe. NMR samples contained 200 μM ^{15}N-enriched $KaiB^{D91R}$ (or $KaiB^{G89A}$) in 350 μL NMR buffer (20 mM Na_2HPO_4/NaH_2PO_4, 100 mM NaCl, 0.02% NaN_3, 10 μM DSS, pH 7.0, 90% H_2O, 10% D_2O). For low-to-high temperature jumps, $KaiB^{D91R}$ (and $KaiB^{G89A}$) samples were stored at –80 °C and incubated at 4 °C for 24 h prior to NMR experiments. Samples were not reused. Series of two-dimensional ^{1}H-^{15}N HSQC spectra were recorded separately at 20 °C, 25 °C, 30 °C, and 35 °C as a function of time upon inserting the 4 °C sample. For temperature jumps to 20 °C and 25 °C, spectra were collected every 0.51 h over a period of 25.5 h. For jumps to 30 °C and 35 °C, spectra were collected every 0.26 h over a period of 13.0 h. For high-to-low temperature jumps, $KaiB^{D91R}$ (and $KaiB^{G89A}$) samples were incubated at 40 °C for 24 h before recording HSQC spectra as a function of time at 20 °C, 25 °C, 30 °C, or 35 °C. ^{1}H chemical shifts were referenced to internal DSS and ^{15}N chemical shifts were indirectly referenced to DSS using absolute frequency ratios listed on the BMRB website. NMR data were processed with NMRPipe and analyzed using nmrDraw or NMRFAM-Sparky (74, 75). See *SI Appendix* for details on data analysis.

NMR HDX Experiments. HDX experiments were initiated by adding 12 °C D_2O to lyophilized ^{15}N-enriched $KaiB^{HDX}$ powder followed by acquisition of ^{15}N, ^{1}H HSQC spectra over a 23-h period at a sample temperature of 12 °C and urea concentrations of 0, 0.5, 1.0, 1.5, 2.0, and 2.5 M urea. Prior to lyophilization, samples were either at pH 5.5 or pH 6.5. HDX rates were determined by fitting HSQC peak heights as a function of time. Under base-catalyzed exchange (pH > 3.5), urea can interfere with HDX and thus we corrected our measured rates accordingly (76). HSQC peaks of slowly exchanging residues can transiently increase in intensity if nearby residues undergo much more rapid HDX (77). Thus, we fit individual HSQC peak intensities, $I(t)$, to the following equation:

$$I(t) = Ae^{-k_{obs}t} - Be^{-k't},$$

where the first term accounts for HDX of the residue in question and the second term accounts for the effect of line narrowing produced by rapid deuteration of nearby residues.

Upside Simulations. We used a near-atomic resolution model called Upside to elucidate fold-switching pathways and their statistics. In Upside simulations, protein conformations are represented by explicit N, C_α, and C atoms, but energies are calculated so as to account for the expected positions of the amide proton, carbonyl oxygen, and an oriented side-chain bead (effectively six atoms per residue) (29, 78, 79). The energy function includes hydrogen bonds, side chain–side chain and side chain–backbone interactions, and desolvation terms, along with trained neighbor- and residue-dependent (ϕ, ψ) dihedral maps. The force field parameters were learned using the contrastive divergence method.

Upside evolves atom positions with Langevin dynamics. A unique feature of the model is that it represents side chain packing probabilistically. As a consequence, side chain packing instantly equilibrates to the backbone conformation at every molecular dynamics (MD) step, which makes each step equivalent to about 30 ps of all-atom dynamics. These elements of the Upside model allow it to describe protein dynamics accurately and rapidly with considerable molecular detail while still generating thermally equilibrated ensembles.

Despite Upside's speed, prohibitively long times are required to observe fold switching in unbiased MD simulations. However, we can obtain statistical information about fold-switching pathways through an approach called the dynamical Galerkin approximation (DGA) (30, 31, 80, 81). In this approach, relatively short unbiased simulations are used to sample portions of the fold-switching pathways, and these data are then used to estimate averages that determine the coefficients of basis expansions of functions of the dynamics, subject to a Markov assumption. Importantly, DGA does not require any single simulation to connect gsKaiB and fsKaiB but simply that the pathways between them are well sampled in aggregate by the short simulations.

In *SI Appendix*, we describe the parameterization of the Upside proline potential, calibration of the Upside temperature, initialization of the Upside simulations, collective variables that we use to characterize the dynamics, details of the DGA calculations, and the Upside HDX analysis.

All-Atom Simulations. We carried out all-atom MD simulations to determine the temperature dependence of the relative free energies of the gsKaiB and fsKaiB conformations. At each temperature from 280 K to 350 K in steps of 5 K, we simulated gsKaiB and fsKaiB for 2 μs and collected the last 1 μs for analysis by MBAR (82). See *SI Appendix* for additional details.

Data, Materials, and Software Availability. The Upside model is available at https://github.com/sosnicklab/upside2-md (79). Analysis scripts for analyzing Upside trajectories are available at https://github.com/dinner-group/KaiB-fold-switching (83). Initial structures of unbiased trajectories, collective variables, and kinetic statistics have been deposited in Zenodo (84).

ACKNOWLEDGMENTS. This work was supported by US NIH grants R35GM-144110 (to A.L.), R35GM136381 (to A.R.D.), R35GM148233 (to T.R.S.), and R35GM141849 (to C.P), NSF Division of Molecular and Cellular Biosciences grants 1953402 (to A.R.D.) and 2023077 (to T.R.S.), NSF Centers of Research Excellence in Science and Technology: Center for Cellular and Biomolecular Machines at the University of California, Merced (NSF-HRD-1547848), and US Army grant W911NF-23-1-0248 (to A.L.). S.C.G. was supported by an NSF Graduate Research Fellowship under Grant No. 2140001. We also acknowledge the Health Sciences Research Institute at UC Merced for pre- and postaward management. We thank Yong-Gang Chang, Archana Chavan, Roger Tseng, Madhurima Das, and Shahar Sukenik for valuable advice, David Rice for NMR support, and Nabil Faruk, Nick Bayhi, and Darren Liu for Upside-related discussions and scripts. This work was completed in part with resources provided by the University of Chicago Research Computing Center and we are grateful for their assistance with the calculations. The "The Beagle-3 cluster used for selected simulations" is supported by the NIH under the High-End Instrumentation grant program award 1S10OD028655-0.

Author affiliations: [a]Department of Chemistry and Biochemistry, University of California, Merced, CA 95343; [b]Department of Chemistry and James Franck Institute, University of Chicago, Chicago, IL 60637; [c]Department of Chemistry, University of California, Davis, CA 95616; [d]Graduate Program in Biophysical Sciences, University of Chicago, Chicago, IL 60637; [e]Department of Biochemistry and Molecular Biology, University of Chicago, Chicago, IL 60637; [f]Department of Chemistry and Biochemistry, University of California, Santa Cruz, CA 95064; and [g]Center for Cellular and Biomolecular Machines, University of California, Merced, CA 95343

Author contributions: N.Z., D.S., N.C., A.A., T.M., S.D., L.H., L.-P.W., T.R.S., A.R.D., and A.L. designed research; N.Z., D.S., S.C.G., N.C., A.A., T.M., Y.X., L.H., M.B., T.R.S., and A.L. performed research; S.D., X.P., and C.P. contributed new reagents/analytic tools; N.Z., D.S., S.C.G., N.C., A.A., T.M., Y.X., L.-P.W., T.R.S., A.R.D., and A.L. analyzed data; and S.C.G., L.-P.W., T.R.S., A.R.D., and A.L. wrote the paper.

1. R. Kolodny, L. Pereyaslavets, A. O. Samson, M. Levitt, On the universe of protein folds. *Annu. Rev. Biophys.* **42**, 559–582 (2013).
2. L. L. Porter, Fluid protein fold space and its implications. *Bioessays* **45**, 2300057 (2023).
3. A. K. Kim, L. L. Porter, Functional and regulatory roles of fold-switching proteins. *Structure* **29**, 6–14 (2021).
4. A. G. Murzin, Metamorphic proteins. *Science* **320**, 1725–1726 (2008).
5. Y.-G. Chang *et al.*, A protein fold switch joins the circadian oscillator to clock output in cyanobacteria. *Science* **349**, 324–328 (2015).
6. R. A. Hut, D. G. M. Beersma, Evolution of time-keeping mechanisms: Early emergence and adaptation to photoperiod. *Philos. Trans. R. Soc. B Biol. Sci.* **366**, 2141–2154 (2011).
7. M. L. Jabbur, C. H. Johnson, Spectres of clock evolution: Past, present, and yet to come. *Front. Physiol.* **12**, 815847 (2022).
8. A. G. Chavan *et al.*, Reconstitution of an intact clock reveals mechanisms of circadian timekeeping. *Science* **374**, eabd4453 (2021).
9. R. Pattanayek *et al.*, Structural model of the circadian clock KaiB–KaiC complex and mechanism for modulation of KaiC phosphorylation. *EMBO J.* **27**, 1767–1778 (2008).
10. R. Iwase *et al.*, Functionally important substructures of circadian clock protein KaiB in a unique tetramer complex. *J. Biol. Chem.* **280**, 43141–43149 (2005).
11. K. Hitomi, T. Oyama, S. Han, A. S. Arvai, E. D. Getzoff, Tetrameric architecture of the circadian clock protein KaiB: A novel interface for intermolecular interactions and its impact on the circadian rhythm. *J. Biol. Chem.* **280**, 19127–19135 (2005).
12. R. G. Garces, N. Wu, W. Gillon, E. F. Pai, Anabaena circadian clock proteins KaiA and KaiB reveal a potential common binding site to their partner KaiC. *EMBO J.* **23**, 1688–1698 (2004).

13. W. Humphrey, A. Dalke, K. Schulten, VMD: Visual molecular dynamics. *J. Mol. Graph.* **14**, 33–38, 27–28 (1996).
14. R. Tseng *et al.*, Structural basis of the day-night transition in a bacterial circadian clock. *Science* **355**, 1174–1180 (2017).
15. M. Rivera, P. Galaz-Davison, I. Retamal-Farfán, E. A. Komives, C. A. Ramírez-Sarmiento, Dimer dissociation is a key energetic event in the fold-switch pathway of KaiB. *Biophys. J.* **121**, 943–955 (2022).
16. R. Tseng *et al.*, Cooperative KaiA–KaiB–KaiC interactions affect KaiB/SasA competition in the circadian clock of cyanobacteria. *J. Mol. Biol.* **426**, 389–402 (2014).
17. Y. Chang, R. Tseng, N. Kuo, A. LiWang, Rhythmic ring-ring stacking drives the circadian oscillator clockwise. *Proc. Natl. Acad. Sci. U.S.A.* **109**, 16847–16851 (2012).
18. G. K. Chow *et al.*, Monitoring protein-protein interactions in the cyanobacterial circadian clock in real time via electron paramagnetic resonance spectroscopy. *Biochemistry* **59**, 2387–2400 (2020).
19. A. Gutu, E. K. O'Shea, Two antagonistic clock-regulated histidine kinases time the activation of circadian gene expression. *Mol. Cell* **50**, 288–294 (2013).
20. S. J. Kim, C. Chi, G. Pattanayak, A. R. Dinner, M. J. Rust, KidA, a multi-PAS domain protein, tunes the period of the cyanobacterial circadian oscillator. *Proc. Natl. Acad. Sci. U.S.A.* **119**, e2202426119 (2022).
21. K. Onai, M. Morishita, S. Itoh, K. Okamoto, M. Ishiura, Circadian rhythms in the thermophilic cyanobacterium *Thermosynechococcus elongatus*: Compensation of period length over a wide temperature range. *J. Bacteriol.* **186**, 4972–4977 (2004).
22. M. Nakajima *et al.*, Reconstitution of circadian oscillation of cyanobacterial KaiC phosphorylation in vitro. *Science* **308**, 414–415 (2005).
23. K. G. Tina, R. Bhadra, N. Srinivasan, PIC: Protein interactions calculator. *Nucleic Acids Res.* **35**, W473–W476 (2007).
24. R. Fraczkiewicz, W. Braun, Exact and efficient analytical calculation of the accessible surface areas and their gradients for macromolecules. *J. Comput. Chem.* **19**, 319–333 (1998).
25. J. K. Myers, C. Nick Pace, J. Martin Scholtz, Denaturant *m* values and heat capacity changes: Relation to changes in accessible surface areas of protein unfolding. *Protein Sci.* **4**, 2138–2148 (1995).
26. E. Van Dijk, A. Hoogeveen, S. Abeln, The hydrophobic temperature dependence of amino acids directly calculated from protein structures. *PLoS Comput. Biol.* **11**, e1004277 (2015).
27. C. L. Dias, T. Ala-Nissila, M. Karttunen, I. Vattulainen, M. Grant, Microscopic mechanism for cold denaturation. *Phys. Rev. Lett.* **100**, 118101 (2008).
28. T. L. Solomon *et al.*, Reversible switching between two common protein folds in a designed system using only temperature. *Proc. Natl. Acad. Sci. U.S.A.* **120**, e2215418120 (2023).
29. J. M. Jumper, N. F. Faruk, K. F. Freed, T. R. Sosnick, Trajectory-based training enables protein simulations with accurate folding and Boltzmann ensembles in cpu-hours. *PLoS Comput. Biol.* **14**, e1006578 (2018).
30. J. Strahan *et al.*, Long-time-scale predictions from short-trajectory data: A benchmark analysis of the Trp-cage miniprotein. *J. Chem. Theory Comput.* **17**, 2948–2963 (2021).
31. E. H. Thiede, D. Giannakis, A. R. Dinner, J. Weare, Galerkin approximation of dynamical quantities using trajectory data. *J. Chem. Phys.* **150**, 244111 (2019).
32. R. B. Best, G. Hummer, W. A. Eaton, Native contacts determine protein folding mechanisms in atomistic simulations. *Proc. Natl. Acad. Sci. U.S.A.* **110**, 17874–17879 (2013).
33. G. S. Hammond, A correlation of reaction rates. *J. Am. Chem. Soc.* **77**, 334–338 (1955).
34. I. E. Sánchez, T. Kiefhaber, Hammond behavior versus ground state effects in protein folding: Evidence for narrow free energy barriers and residual structure in unfolded states. *J. Mol. Biol.* **327**, 867–884 (2003).
35. H. Taskent, J.-H. Cho, D. P. Raleigh, Temperature-dependent Hammond behavior in a protein-folding reaction: Analysis of transition-state movement and ground-state effects. *J. Mol. Biol.* **378**, 699–706 (2008).
36. Y. Bai, T. Sosnick, L. Mayne, S. Englander, Protein folding intermediates: Native-state hydrogen exchange. *Science* **269**, 192–197 (1995).
37. B. M. P. Huyghues-Despointes, C. N. Pace, S. W. Englander, J. M. Scholtz, "Measuring the conformational stability of a protein by hydrogen exchange" in *Protein Structure, Stability, and Folding*, K. P. Murphy, Ed. (Humana Press, 2001), pp. 69–92.
38. I. Vakonakis, D. A. Klewer, S. B. Williams, S. S. Golden, A. C. LiWang, Structure of the N-terminal domain of the circadian clock-associated histidine kinase SasA. *J. Mol. Biol.* **342**, 9–17 (2004).
39. C. L. Gustafson *et al.*, A slow conformational switch in the BMAL1 transactivation domain modulates circadian rhythms. *Mol. Cell* **66**, 447–457.e7 (2017).
40. A. H. Andreotti, Native state proline isomerization: An intrinsic molecular switch. *Biochemistry* **42**, 9515–9524 (2003).
41. K. P. Lu, G. Finn, T. H. Lee, L. K. Nicholson, Prolyl cis-trans isomerization as a molecular timer. *Nat. Chem. Biol.* **3**, 619–629 (2007).
42. G. Schoetz, O. Trapp, V. Schurig, Determination of the cis-trans isomerization barrier of several L-peptidyl-L-proline dipeptides by dynamic capillary electrophoresis and computer simulation. *Electrophoresis* **22**, 2409–2415 (2001).
43. M. Shibukawa, A. Miyake, S. Eda, S. Saito, Determination of the cis–trans isomerization barriers of L-alanyl-L-proline in aqueous solutions and at water/hydrophobic interfaces by on-line temperature-jump relaxation HPLC and dynamic on-column reaction HPLC. *Anal. Chem.* **87**, 9280–9287 (2015).
44. E. S. Eberhardt, N. Panasik, R. T. Raines, Inductive effects on the energetics of prolyl peptide bond isomerization: Implications for collagen folding and stability. *J. Am. Chem. Soc.* **118**, 12261–12266 (1996).
45. A. Antoszewski, "Enhanced sampling and dynamical analyses of multipathway reactions: Applications to insulin and KaiB," Dissertation, The University of Chicago, Chicago, IL (2022).
46. W. Kabsch, C. Sander, Dictionary of protein secondary structure: Pattern recognition of hydrogen-bonded and geometrical features. *Biopolymers* **22**, 2577–2637 (1983).
47. P. Wang, J. Heitman, The cyclophilins. *Genome Biol.* **6**, 226 (2005).
48. D. A. Bosco, E. Z. Eisenmesser, S. Pochapsky, W. I. Sundquist, D. Kern, Catalysis of cis/trans isomerization in native HIV-1 capsid by human cyclophilin A. *Proc. Natl. Acad. Sci. U.S.A.* **99**, 5247–5252 (2002).
49. P. Sarkar, C. Reichman, T. Saleh, R. B. Birge, C. G. Kalodimos, Proline *cis–trans* isomerization controls autoinhibition of a signaling protein. *Mol. Cell* **25**, 413–426 (2007).
50. A. S. Holehouse, B. B. Kragelund, The molecular basis for cellular function of intrinsically disordered protein regions. *Nat. Rev. Mol. Cell Biol.* **25**, 187–211 (2024), 10.1038/s41580-023-00673-0.
51. D. Willbold, B. Strodel, G. F. Schröder, W. Hoyer, H. Heise, Amyloid-type protein aggregation and prion-like properties of amyloids. *Chem. Rev.* **121**, 8285–8307 (2021).
52. E. K. Jaffe, Morpheeins–A new structural paradigm for allosteric regulation. *Trends Biochem. Sci.* **30**, 490–497 (2005).
53. C. J. Jeffery, Moonlighting proteins. *Trends Biochem. Sci.* **24**, 8–11 (1999).
54. H. K. Wayment-Steele *et al.*, Predicting multiple conformations via sequence clustering and AlphaFold2. *Nature* **625**, 832–839 (2023), 10.1038/s41586-023-06832-9.
55. N. Chen, M. Das, A. LiWang, L.-P. Wang, Sequence-based prediction of metamorphic behavior in proteins. *Biophys. J.* **119**, 1380–1390 (2020).
56. S. Mishra, L. L. Looger, L. L. Porter, Inaccurate secondary structure predictions often indicate protein fold switching. *Protein Sci.* **28**, 1487–1493 (2019).
57. R. Mutoh, H. Mino, R. Murakami, T. Uzumaki, M. Ishiura, Thermodynamically induced conformational changes of the cyanobacterial circadian clock protein KaiB. *Appl. Magn. Reson.* **40**, 525–534 (2011).
58. T. Iida *et al.*, Importance of the monomer-dimer-tetramer interconversion of the clock protein KaiB in the generation of circadian oscillations in cyanobacteria. *Genes Cells* **20**, 173–190 (2015), 10.1111/gtc.12211.
59. J. Snijder *et al.*, Structures of the cyanobacterial circadian oscillator frozen in a fully assembled state. *Science* **355**, 1181–1184 (2017).
60. W. Pitsawong *et al.*, From primordial clocks to circadian oscillators. *Nature* **616**, 183–189 (2023).
61. M. Loza-Correa *et al.*, The Legionella pneumophila kai operon is implicated in stress response and confers fitness in competitive environments. *Environ. Microbiol.* **16**, 359–381 (2013).
62. G. K. Chow *et al.*, A night-time edge site intermediate in the cyanobacterial circadian clock identified by EPR spectroscopy. *J. Am. Chem. Soc.* **144**, 184–194 (2022).
63. B. Novak, J. J. Tyson, Design principles of biochemical oscillators. *Nat. Rev. Mol. Cell Biol.* **9**, 981–991 (2008).
64. R. K. Barrett, J. S. Takahashi, Temperature compensation and temperature entrainment of the chick pineal cell circadian clock. *J. Neurosci.* **15**, 5681–5692 (1995).
65. J.-C. Leloup, A. Goldbeter, Temperature compensation of circadian rhythms: Control of the period in a model for circadian oscillations of the per protein in Drosophila. *Chronobiol. Int.* **14**, 511–520 (1997).
66. R. Murakami *et al.*, ATPase activity and its temperature compensation of the cyanobacterial clock protein KaiC. *Genes Cells* **13**, 387–395 (2008).
67. A. Mehra *et al.*, A role for casein kinase 2 in the mechanism underlying circadian temperature compensation. *Cell* **137**, 749–760 (2009).
68. K. Terauchi *et al.*, ATPase activity of KaiC determines the basic timing for circadian clock of cyanobacteria. *Proc. Natl. Acad. Sci. U.S.A.* **104**, 16377–16381 (2007).
69. H. K. Wayment-Steele *et al.*, The conformational landscape of fold-switcher KaiB is tuned to the circadian rhythm timescale. *Proc. Natl. Acad. Sci. U.S.A.* 121, e2412293121.
70. S. Akiyama, A. Nohara, K. Ito, Y. Maeda, Assembly and disassembly dynamics of the cyanobacterial periodosome. *Mol Cell* **29**, 703–716 (2008).
71. N. Zhang, W. Guan, S. Cui, N. Ai, Crowded environments tune the fold-switching in metamorphic proteins. *Commun. Chem.* **6**, 1–7 (2023).
72. A. Chavan *et al.*, Protocols for in vitro reconstitution of the cyanobacterial circadian clock. *Biopolymers* **115**, e23559 (2024).
73. J. Heisler, A. Chavan, Y.-G. Chang, A. LiWang, Real-time in vitro fluorescence anisotropy of the cyanobacterial circadian clock. *Methods Protoc.* **2**, 42 (2019).
74. F. Delaglio *et al.*, NMRPipe: A multidimensional spectral processing system based on UNIX pipes. *J. Biomol. NMR* **6**, 277–293 (1995).
75. W. Lee, M. Tonelli, J. L. Markley, NMRFAM-SPARKY: Enhanced software for biomolecular NMR spectroscopy. *Bioinformatics* **31**, 1325–1327 (2015).
76. D. Loftus, G. O. Gbenle, P. S. Kim, R. L. Baldwin, Effects of denaturants on amide proton exchange rates: A test for structure in protein fragments and folding intermediates. *Biochemistry* **25**, 1428–1436 (1986).
77. M. Xue, R. Kitahara, Y. Yoshimura, F. A. A. Mulder, Aberrant increase of NMR signal in hydrogen exchange experiments. Observation and explanation. *Biochem. Biophys. Res. Commun.* **478**, 1185–1188 (2016).
78. J. M. Jumper, N. F. Faruk, K. F. Freed, T. R. Sosnick, Accurate calculation of side chain packing and free energy with applications to protein molecular dynamics. *PLoS Comput. Biol.* **14**, e1006342 (2018).
79. X. Peng *et al.*, Prediction and validation of a protein's free energy surface using hydrogen exchange and (importantly) its denaturant dependence. *J. Chem. Theory Comput.* **18**, 550–561 (2022).
80. S. C. Guo, R. Shen, B. Roux, A. R. Dinner, Dynamics of activation in the voltage-sensing domain of Ci-VSP. *Nat. Commun.* **15**, 1408 (2024).
81. A. Antoszewski, C. Lorpaiboon, J. Strahan, A. R. Dinner, Kinetics of phenol escape from the insulin R_6 hexamer. *J. Phys. Chem. B* **125**, 11637–11649 (2021).
82. M. R. Shirts, J. D. Chodera, Statistically optimal analysis of samples from multiple equilibrium states. *J. Chem. Phys.* **129**, 124105 (2008).
83. S. C. Guo, Temperature-dependent fold-switching mechanism of the circadian clock protein KaiB. Github. https://github.com/dinner-group/KaiB-fold-switching. Deposited 17 September 2024.
84. S. C. Guo, Temperature-dependent fold-switching mechanism of the circadian clock protein KaiB. Zenodo. https://doi.org/10.5281/zenodo.14160033. Deposited 13 November 2024.